UDK 620.1:544.227:543.316/.318:67.017
Original scientific article/Izvirni znanstveni članek

ISSN 1580-2949
MTAEC9, 53(6)891(2019)

EFFECT OF MANGANESE DOPING ON THE MAGNETIC AND MAGNETOCALORIC PROPERTIES OF ZINC FERRITE

VPLIV DOPIRANJA Z Mn NA MAGNETNE IN MAGNETNO-KALORIČNE LASTNOSTI Zn FERITA

Haitao Zhao*, Xuehan Li, Hui Zhao, Yulian Wang

School of Materials Science and Engineering, Shenyang Ligong University, Shenyang, China

Prejem rokopisa – received: 2019-04-26; sprejem za objavo – accepted for publication: 2019-07-23

doi:10.17222/mit.2019.089

$Mn_xZn_{1-x}Fe_2O_4$ ferrites with x = 0.2, 0.4, 0.6 and 0.8 were successfully prepared with the solvothermal method. The structural characteristics, morphology and magnetic properties of the composite powders were obtained with X-ray diffraction (XRD), a scanning electron microscope (SEM) and a vibrating-sample magnetometer (VSM). The results show that $Mn_xZn_{1-x}Fe_2O_4$ ferrite has a pure cubic spinel structure with a particle size of about 200–300 nm. Ethylene glycol plays an important role during the formation of monodisperse particles. Synthesized particles exhibit ferromagnetic behavior with a small hysteresis at room temperature. Ms reaches the maximum value of 71.99 emu/g when the amount of manganese ions is x = 0.6. At 600 s, the temperature of $Mn_{0.8}Zn_{0.2}Fe_2O_4$ can rise to 69.9 °C, showing an excellent magnetocaloric effect.

Keywords: zinc ferrite, solvothermal synthesis, magnetic properties, magnetocaloric effect

Avtorji so uspešno sintetizirali $Mn_xZn_{1-x}Fe_2O_4$ ferite z x = 0,2, 0,4, 0,6 in 0,8 s solvotermalno metodo. Z rentgensko difrakcijo (XRD), vrstično elektronsko mikroskopijo (SEM) in magnetometrom na tresoči se vzorec (VSM), so določili strukturne lastnosti, morfologijo in magnetne lastnosti kompozitnih prahov. Rezultati analiz so pokazali, da ima $Mn_xZn_{1-x}Fe_2O_4$ ferit čisto kubično-špinelno strukturo z velikostjo delcev okoli 200 nm do 300 nm. Etilenglikol igra pomembno vlogo pri tvorbi enovite disperzije delcev ferita. Sintetizirani delci imajo feromagnetne lastnosti z majhno histerezo pri sobni temperaturi. Maksimalna vrednost magnetizacije nasičenja (Ms) je bila 71,99 emu/g pri vsebnosti Mn ionov x = 0,6. Po 600 s temperatura $Mn_{0.8}Zn_{0.2}Fe_2O_4$ lahko naraste do 69,9 °C, kar kaže na odličen magnetno-kaloričen učinek.

Ključne besede: cink-ferit, solvotermalna sinteza, magnetne lastnosti, magnetno-kalorično delovanje

1 INTRODUCTION

MnZn ferrites attracted considerable investigations because of their potential applications in catalysis, magnetic storage, cancer therapy, medical imaging and electronic devices.[1–5] The chemical processes currently in vogue for the synthesis of MnZn ferrite particles include co-precipitation,[6–9] the sol–gel auto-combustion method,[10–13] the solid-state reaction method,[14–16] solvothermal technique,[17–19] microwave processing technique,[20–22] hydrothermal synthesis etc.[23–27]

The solvothermal technique has the advantages of functioning at low temperatures, being a simple, low-cost synthetic process, exhibiting an ease of compositional control and producing ultrafine particles with a narrow-sized distribution. Therefore, the solvothermal technique is an economical and simple strategy for the synthesis of monodisperse powders. G. S. Wang et al.[28] successfully prepared $ZnFe_2O_4$ nanocrystal clusters with a surfactant-assisted solvothermal method and investigated them as a potential magnetorheological material. W. Shen et al.[29] demonstrated a simple solvothermal route for the synthesis of monodisperse Fe_3O_4 and studied the effects of the reaction parameters on the structure. However, their investigations focused on structural, magnetic and electrical properties at lower frequencies (<1 GHz). Until now, there has been little research work on the magnetic properties and magnetocaloric effect of MnZn ferrites. In the present study, monodispersed $Mn_xZn_{1-x}Fe_2O_4$ (x = 0.2, 0.4, 0.6 and 0.8) ferrite particles were synthesized using a solvothermal approach. The samples were characterized with various experimental techniques and the properties of ferrite particles were investigated.

2 EXPERIMENTAL PART

$Mn_xZn_{1-x}Fe_2O_4$ (x = 0.2, 0.4, 0.6 and 0.8) ferrite particles were synthesized using a solvothermal approach. Analytical-grade $FeCl_3{\cdot}6H_2O$, $Zn(NO_3)_2{\cdot}6H_2O$ and $MnSO_4{\cdot}H_2O$ were used to prepare ferrite powders. The metal salt, weighed according to the stoichiometric proportion, was dissolved evenly in ethylene glycol to obtain a homogeneous solution. After that, the resulting mixture was transferred into a 100-mL Teflon-lined stainless-steel autoclave, and heated to 200 °C for 12 h. The system was then cooled down to room temperature. The products were obtained with centrifugation, sequentially washed with deionized water and ethanol

*Corresponding author's e-mail:
zht95711@163.com (Haitao Zhao)

for several times and then dried in a vacuum oven at 60 °C for 12 h.

The phase formation of the synthesized product was identified with X-ray diffraction (XRD, Ultima IV, Rigaku, Japan) using Cu-K_α radiation (λ = 0.15418 nm) in a 2θ range of 20–70°. The morphology of the products was observed with a scanning electron microscope (SEM) on an S-3400N microscope operating at 25 kV. Their magnetic properties were measured with a Lake Shore 7410 vibrating-sample magnetometer (VSM) at room temperature.

3 RESULTS

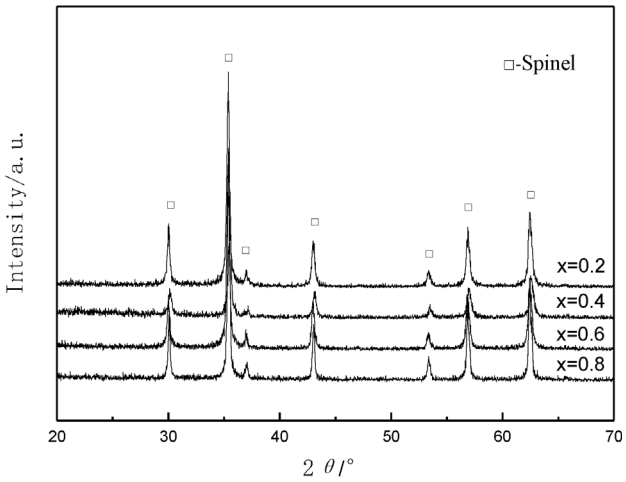

Figure 1: XRD patterns of $Mn_xZn_{1-x}Fe_2O_4$ ferrites

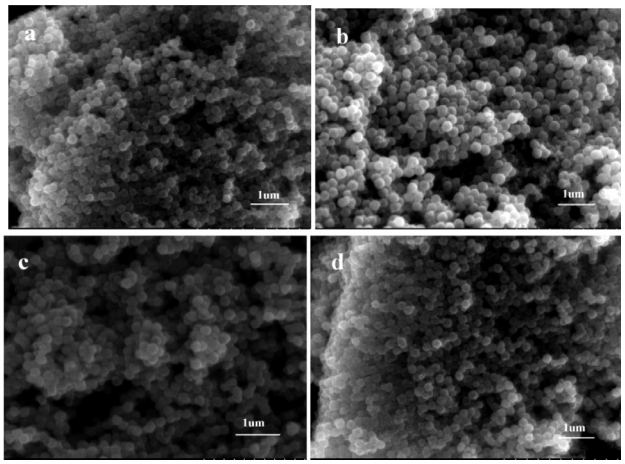

Figure 2: SEM images of $Mn_xZn_{1-x}Fe_2O_4$ particles: a) x = 0.2, b) x = 0.4, c) x = 0.6, d) x = 0.8

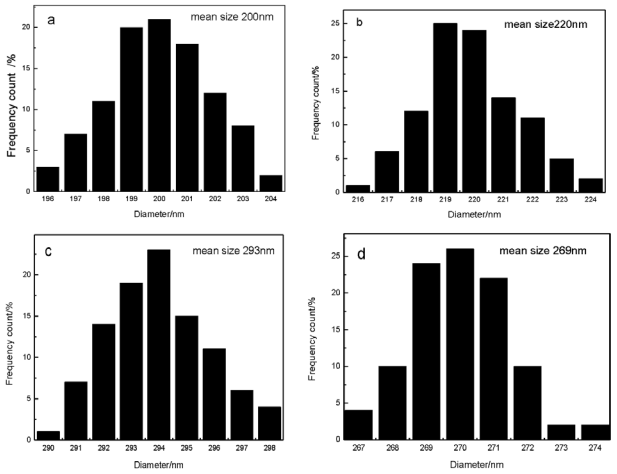

Figure 3: Particle-size distributions of $Mn_xZn_{1-x}Fe_2O_4$ ferrites: a) x = 0.2, b) x = 0.4, c) x = 0.6, d) x = 0.8

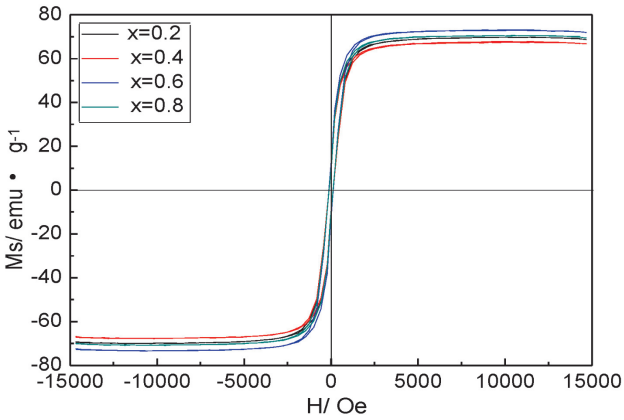

Figure 4: Hysteresis loops of $Mn_xZn_{1-x}Fe_2O_4$ nanoparticles at room temperature (300 K)

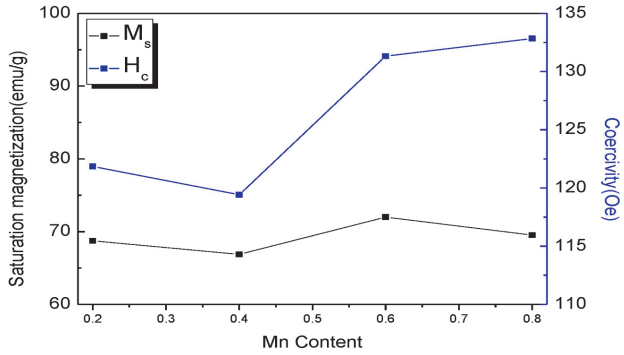

Figure 5: Curves of Mn amounts in Ms and Hc

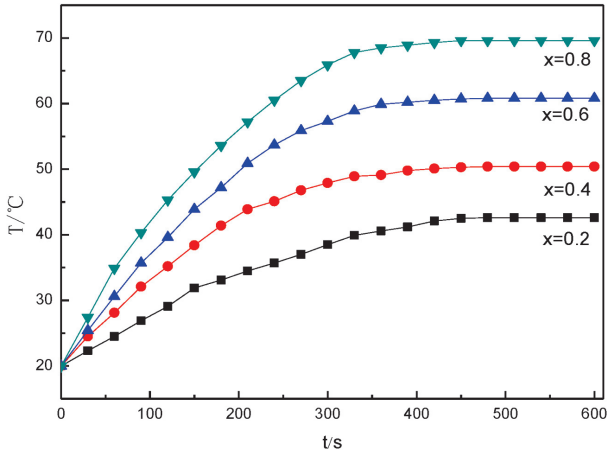

Figure 6: Time-temperature curves of $Mn_xZn_{1-x}Fe_2O_4$ particles

Table 1: Main magnetic properties of $Mn_xZn_{1-x}Fe_2O_4$ particles

Formula	M_s (emu/g)	M_r (emu/g)	H_c (Oe)	μ_B
$Mn_{0.2}Zn_{0.8}Fe_2O_4$	66.87	10.35	119.42	2.88
$Mn_{0.4}Zn_{0.6}Fe_2O_4$	68.73	10.90	121.85	2.94
$Mn_{0.6}Zn_{0.4}Fe_2O_4$	71.99	12.36	131.32	3.03
$Mn_{0.8}Zn_{0.2}Fe_2O_4$	69.53	10.30	132.84	2.91

4 DISCUSSION

To identify the phase change, the XRD patterns of $Mn_xZn_{1-x}Fe_2O_4$ with x = 0.2, 0.4, 0.6 and 0.8 are shown in **Figure 1**. The positions and relative intensities of all diffraction peaks are assigned to the (111), (220), (311), (400), (511), (440) and (533) reflections of those from the JCPDS card (No.73-1963) for $Mn_xZn_{1-x}Fe_2O_4$. Sharp and strong peaks confirm the obtained powders have a single-phase cubic spinel structure. The average crystal size (D) for each sample is estimated from the diffraction data for the (311) plane from the XRD patterns, in accordance with the Debye-Scherrer formula in Equation (1):

$$D = \frac{0.89\lambda}{\beta \cos\theta} \quad (1)$$

where λ is the X-ray wavelength, β is the value of the full width at half maximum (FWHM) of the (311) diffraction peak, and θ is the Bragg angle of the (311) peak. The average crystal size of $Mn_xZn_{1-x}Fe_2O_4$ ferrites, as deduced from the X-ray data, is in a range of 205 nm to 287 nm for all the samples. There is a systematic increase in the crystal size with the increase in the Mn concentration. This phenomenon suggests that the Mn^{2+} ion doping influences the particle crystallization during the solvothermal process and promotes the grain growth of crystallite Zn^{2+} owing to crystal-lattice inflations.

SEM images of the $Mn_{1-x}Zn_xFe_2O_4$ particles are shown in **Figure 2**. It reveals that the obtained particles demonstrate the high quality and uniformity of the particle size. The particles are monodisperse, exhibiting a spherical shape with a narrow-sized distribution. These particles have an average size of about 200–300 nm. Ethylene glycol plays an important role during the formation of monodisperse particles, which can slow down the aggregation growth of crystals due to fewer surface hydroxyls and a higher viscosity of the system, providing enough time for the powders to rotate adequately, finding a suitable configuration interface.

Particle-size distribution of the $Mn_{1-x}Zn_xFe_2O_4$ particles is shown in **Figure 3**. It reveals that the average particle sizes of x = 0.2, 0.4, 0.6 and 0.8 are (200, 220, 293 and 269) nm, respectively. The statistical results are basically consistent with the XRD analysis. In **Figure 3a**, less than 5 % of the samples is taken up by the total particle sizes of 198 nm and 204 nm, while (20.05, 22.13 and 18.72) % of the samples are taken up by the sizes of (199, 200 and 201) nm, respectively. The combined proportion of the three is 60.90 %. In **Figure 3b**, the proportions of the particles of 219 nm and 220 nm are 25.12 % and 23.34 %, respectively; both values together amount to 48.46 %, while the other-size particles amount to 50 %. In **Figure 3c**, the particles of 291 nm, and 298 nm account for less than 5 % of the samples, while the particles of (293, 294 and 295) nm account for about 60 % of the samples. The particle size of the prepared samples is basically between 293 nm and 295 nm. It can be concluded that the particle-size distribution of the prepared samples is relatively wide. In **Figure 3d**, about 73 % of the particles were (269, 270 and 271) nm. It can be seen that the particle size of the synthesized powders is uniform and the distribution is concentrated when x = 0.8. As can be seen from **Figure 3**, the proportion of the particulate matter can reach about 25 % in some samples, while in other samples, it is less than 5 %. The particle spacing is quite different, and the zinc ion content has a certain influence on the particle size of the product. In summary, different stoichiometric ratios are closely related to the particle size and particle distribution. In order to obtain products with a smaller particle-size difference, it is necessary to adjust the ratio of manganese and zinc ions in the reaction system.

The magnetic properties of $Mn_xZn_{1-x}Fe_2O_4$ ferrites were studied using a vibrating-sample magnetometer at room temperature. In **Figure 4**, it can be observed that Mn-Zn ferrites synthesized at different molar ratios show ferromagnetic properties because the residual saturation magnetization and coercivity are small at room temperature. The corresponding magnetic properties of $Mn_xZn_{1-x}Fe_2O_4$ are shown in **Table 1**. **Figure 5** shows the variation trend of the saturation magnetization (Ms) and coercivity (Hc) with different amounts of manganese ions. It can be observed that Ms reaches the maximum value of 71.99 emu/g when the amount of manganese ions is x = 0.6, and the coercivity curve first shows a decreasing trend and then an increase with the increase in the amount of manganese ions. When x = 0.8, the

coercivity is 131.84 Oe. This phenomenon shows that the saturation magnetization and coercivity of manganese-zinc ferrite are closely related to the substitution degree of zinc ions for a constant external magnetic field. With the increase in the Mn^{2+} addition, the degree of substitution for Zn^{2+} increases, and the saturation magnetization of the product continues to increase. If $x > 0.6$, the degree of substitution for Zn^{2+} gradually decreases.

With the increasing concentration of manganese ions, manganese ions preferentially occupy the octahedral B site, which results in an equal number of trivalent iron ions entering the tetrahedral A site. In the Néel model, the magnetic moment $\mu_B(\chi)$ can be expressed with the following Equation (2):

$$\mu_B(\chi) = M_B(\chi) - M_A(\chi) \quad (2)$$

In this formula, M_A and M_B represent the magnetic moments of the tetrahedral structure position (A) and octahedral structure position (B) in the Mn-Zn ferrite, respectively. The magnetic moment μ_B is closely related to the structure position, the distribution of metal cations and the spin/tilt effect. As the concentration of Mn^{2+} gradually increases, the corresponding magnetic moment μ_B first increases and then decreases. This is because when the amount of Mn^{2+} is relatively small, Mn^{2+} can preferentially occupy position B of the octahedron structure, which forces the same amount of Fe^{3+} in the reaction system to enter position A of the tetrahedron structure. This results in a gradual increase in the super-exchange force between A–B sites, net magnetic moment and saturation magnetization Ms. When the amount of Mn^{2+} exceeds 0.4, the A–B exchange force begins to weaken, while the B–B exchange force increases. As the content of manganese ions increases continuously and occupies the B position, the redundant part of Mn^{2+} enters the tetrahedron-to-tetrahedron structure position so that the same amount of Fe^{3+} in the tetrahedron gap returns to the octahedron structure position, resulting in an increase in the magnetic moment of the B position. This rearrangement rapidly increases the exchange force of the B–B position, forcing the number of reverse parallel-spin coupling pairs in the octahedron gap to increase continuously so that the saturation-magnetization intensity is decreased. μ_B is the experimental value of the magnetic moment of the ferrite which can be calculated with the following formula in Equation (3):

$$\mu_B = \frac{M \times M_s}{5585} \quad (3)$$

μ_B – experimental value of the magnetic moment;
M – molar molecular mass;
M_s – saturation magnetization.

According to Equation (3), the calculation results for μ_B are listed in **Table 1**. From **Table 1**, it can be concluded that the values of the magnetic moment and saturation magnetization are closely related, and μ_B is proportional to *Ms*.

Figure 6 is a time-temperature curve of the $Mn_xZn_{1-x}Fe_2O_4$ particles under a 50-kHz external alternating magnetic field. It can be seen from **Figure 6** that $Mn_xZn_{1-x}Fe_2O_4$ can convert part of the electromagnetic energy into internal energy under the action of an external alternating magnetic field, which can increase the temperature of the product. When x = 0.2, 0.4, 0.6 and 0.8, the final temperatures can reach (42.5, 50.4, 60.8 and 69.9) °C, respectively. In the period of 0–200 s, the rate of the temperature rise is fast, but during the period of 200–400 s, it is slower. The temperature of the product during the period of 400–600 s is no longer on the increase, gradually reaching a stable value. This is because the heat production and environmental-heat dissipation of the sample are in a relative equilibrium state and the heat is no longer diffused.

The increase in the product temperature is closely related to its magnetic loss, which consists of the eddy current loss, hysteresis loss and residual loss. As the Mn-Zn ferrite synthesized with the solvothermal method has a high resistivity, the effects of the eddy current loss and residual loss on the energy conversion can be neglected, so the final heat of the prepared product is closely related to the hysteresis loss. When the power of the applied magnetic field is fixed to a certain value, the heat generated by the hysteresis loss can be indirectly expressed by the product of the saturation magnetization, M_s, and the coercivity, Hc. When x = 0.8, the product of the saturated magnetization and coercivity reaches the maximum value, also indicating the fastest heating rate under the alternating magnetic field, and the temperature of the sample reaches the highest value. At 600 s, the temperature can rise to 69.9 °C, showing an excellent magnetocaloric effect.

5 CONCLUSIONS

$Mn_xZn_{1-x}Fe_2O_4$ particles constitute a single-phase cubic spinel structure. Synthesized $Mn_xZn_{1-x}Fe_2O_4$ particles are spherical and have good crystallinity. With an increase in the manganese ion amount, the particle size of the product first increased and then decreased. $Mn_xZn_{1-x}Fe_2O_4$ powders show ferromagnetism. As the x-value gradually increased, the Ms of the product first increased and then decreased. The maximum value was 71.99 emu/g at x = 0.6. Manganese-zinc ferrites with different molar ratios lasted 600 seconds under a 50-kHz alternating magnetic field, and the temperature of the mixed dispersion solution of the samples could reach 42.5–69.9 °C. With an increase in the x-value, the magnetocaloric properties of the Mn-Zn ferrite improved significantly, which was closely related to the hysteresis-loop area and the hysteresis power loss of the product.

Acknowledgment

This work was financially supported by National Natural Science Foundation of China (51303108) and National Equipment Pre-research Project of China (61409230605) .

6 REFERENCES

[1] R. P. Araújo-Neto, E. L. Silva-Freitas, J. F. Carvalho, T. R. F. Pontes, K. L. Silva, I. H. M. Damasceno, E. S. T. Egito, A. L. Dantas, M. A. Morales, A. S. Carriço, , Monodisperse sodium oleate coated magnetite high susceptibility nanoparticles for hyperthermia applications, Journal of Magnetism and Magnetic Materials, 364 (**2014**), 72–79, doi:10.1016/j.jmmm.2014.04.001

[2] V. Tsakaloudi, D. Holz, V. Zaspalis, The effect of externally applied uniaxial compressive stress on the magnetic properties of power MnZn-ferrites, J. Mater. Sci., 48 (**2013**), 3825–3833, doi:10.1007/s10853-013-7183-2

[3] D. G. Li, C. Chen, W. Rao, W. H. Lu, Y. H. Xiong, Preparation and microwave absorption properties of polyaniline/$Mn_{0.8}Zn_{0.2}Fe_2O_4$ nanocomposite in 2-18 GHz, J. Mater. Sci.: Mater. Electron., 25 (**2014**), 76–81, doi:10.1007/s10854-013-1551-1

[4] Q. Zhang, P. Zheng, L. Zheng, J. Zhou, H. Qin, Effect of Co-substitution on the structure and magnetic properties of MnZn power ferrite, J. Electroceram., 32 (**2014**), 230–233, doi:10.1007/s10832-013-9878-9

[5] W. J. Wang, C. G. Zang, Q. J. Jiao, Synthesis, structure and electromagnetic properties of Mn–Zn ferrite by sol-gel combustion technique, Journal of Magnetism and Magnetic Materials, 349 (**2014**), 116–120, doi:10.1016/j.jmmm.2013.08.057

[6] C. H. Dong, G. X. Wang, L. Shi, D. W. Guo, C. J. Jiang, D. S. Xue, Investigation of the thermal stability of Mn ferrite particles synthesized by a modified co-precipitation method, Science China: Physics, Mechanics & Astronomy, 56 (**2013**) 3, 568–572, doi:10.1007/s11433-012-4885-4

[7] K. Rana, P. Thakur, M. Tomar, V. Gupta, A. Thakur, Investigation of cobalt substituted M-type barium ferrite synthesized via co-precipitation method for radar absorbing material in Ku-band (12–18 GHz), Ceramics International, 44 (**2018**) 6, 6370–6375, doi:10.1016/j.ceramint.2018.01.028

[8] T. M. Hammad, J. K. Salem, A. A. Amsha, N. K. Hejazy , Optical and magnetic characterizations of zinc substituted copper ferrite synthesized by a co-precipitation chemical method, Journal of Alloys and Compounds, 741 (**2018**), 123–130, doi:10.1016/j.jallcom.2018.01.123

[9] V. Manikandan, X. Li, R. S. Mane, J. Chandrasekaran, Room temperature gas sensing properties of sn-substituted nickel ferrite ($NiFe_2O_4$) thin film sensors prepared by chemical co-precipitation method, Journal of Electronic Materials, 47 (**2018**) 7, 3403–3408, doi:10.1007/s11664-018-6295-5

[10] M. R. Barati, Characterization and preparation of nanocrystalline MgCuZn ferrite powders synthesized by sol–gel auto-combustion method, J. Sol-Gel Sci. Technol., 52 (**2009**), 171–178, doi:10.1007/s10971-009-2023-1

[11] J. L. Liu, M. Yang, S. Y. Wang, J. Q. Lv, Y.Li, M. Zhang, Sol-gel auto-combustion synthesis and properties of Co_2 Z-type hexagonal ferrite ultrafine powders, Journal of Magnetism and Magnetic Materials, 454 (**2018**), 1–5, doi:10.1016/j.jmmm.2018.01.049

[12] N. Yasmin, I. Inam, M. Iftikhar, M. Zahid, M. N. Ashiq, S. Abdulsatar, M. Safdar, M. Mirza, Structural and magnetic properties of Cr doped strontium spinel ferrite $SrFe_2O_4$ by sol-gel auto-combustion method, Physica B: Condensed Matter, 550 (**2018**), 90–95, doi:10.1016/j.physb.2018.08.039

[13] B. H. Guan, M. H. Zahari, K. C. Lee, Effect of La^{3+} substitution on the structural and magnetic properties of Mn-Zn ferrite prepared by sol-gel auto-combustion method, Materials Science Forum, 916 (**2018**), 91–95, doi:10.4028/www.scientific.net/MSF.916.91

[14] E. M. Ibrahim, The effect of sintering time and temperature on the electrical properties of MnZn ferrites, Appl. Phys. A, 89 (**2007**), 203–208, doi:10.1007/s00339-007-4088-4

[15] M. Mashadi, Y. Yunasfi, A. Mulyawan, Microwave absorption study of manganese ferrite in X-band range prepared by solid state reaction method, Jurnal Teknologi, 80 (**2018**) 2, 147–151, doi:10.11113/jt.v80.10773

[16] G. P. Kumar, V. Raghavendra, C. P. Babu, Synthesis, structural studies on Ni-Zn ferrite by solid state reaction method, Chemical Science Transactions, 5 (**2016**) 4, 1096–1099, doi:10.7598/cst2016.1311

[17] S. Surinwong, A. Rujiwatra, Ultrasonic cavitation assisted solvothermal synthesis of superparamagnetic zinc ferrite nanoparticles, Particuology, 11 (**2013**), 588–593, doi:10.1016/j.partic.2012.06.008

[18] A. Kalam, A. G. Al-Sehemi, M. Assiri, G. Du, T. Ahmad, I. Ahmad, M. Pannipara, Modified solvothermal synthesis of cobalt ferrite ($CoFe_2O_4$) magnetic nanoparticles photocatalysts for degradation of methylene blue with H_2O_2/visible light, Results in Physics, 8 (**2018**), 1046–1053, doi:10.1016/j.rinp.2018.01.045

[19] K. Muthukumar, D. S. Lakshmi, S. D. Acharya, S. Natarajan, A. Mukherjee, H. C. Bajaj, Solvothermal synthesis of magnetic copper ferrite nano sheet and its antimicrobial studies, Materials Chemistry and Physics, 209 (**2018**), 172–179, doi:10.1016/j.matchemphys.2018.02.004

[20] S. Thota, S. C. Kashyap, H. C. Gupta, T. K. Nath, Improved Magnetic Properties of Microwave-Processed $Mn_{0.5}Zn_{0.5}Fe_2O_4$ Nanoparticles, J. Supercond. Nov. Magn., 28 (**2015**), 131–136, doi:10.1007/s10948-014-2820-9

[21] V. K. Sankaranarayanan, C. Sreekumar, Precursor synthesis and microwave processing of nickel ferrite nanoparticles, Current Applied Physics, 3 (**2003**), 205–208, doi:10.1016/S1567-1739(02)00202-X

[22] C.l E. Patton, M. Z. Wu, K. R. Smith, V. I. Vasyuchka, Nonlinear ferrite film microwave signal processing for advanced communications-physics and devices, Ferroelectrics, 342 (**2006**) 1, 101–106, doi:10.1080/00150190600946260

[23] K. V. Sankar, S. Shanmugapriya, S. Surendran, S. C. Jun, R. K.Selvan, Facile hydrothermal synthesis of carbon-coated cobalt ferrite spherical nanoparticles as a potential negative electrode for flexible supercapattery, Journal of Colloid and Interface Science, 513 (**2018**), 480–488, doi:10.1016/j.jcis.2017.11.054

[24] M. Q. Hua, L. Xu, F. Cui, J. Lian, Y. Huang, J. Bao, J. Qiu, Y. Xu, H. Xu, Y. Zhao, H.Li, Hexamethylenetetramine-assisted hydrothermal synthesis of octahedral nickel ferrite oxide nanocrystallines with excellent supercapacitive performance, Journal of Materials Science, 53 (**2018**) 10, 7621–7636, doi:10.1007/s10853-018-2052-7

[25] S. Y. Liu, L. Y. Wang, K. C. Chou, Synthesis of metal-doped Mn-Zn ferrite from the leaching solutions of vanadium slag using hydrothermal method, Journal of Magnetism and Magnetic Materials, 449 (**2018**), 49–54, doi:10.1016/j.jmmm.2017.10.001

[26] R. S. Melo, P. Banerjee, A. Franco, Hydrothermal synthesis of nickel doped cobalt ferrite nanoparticles: optical and magnetic properties, Journal of Materials Science: Materials in Electronics, 29 (**2018**), 14657–14667, doi:10.1007/s10854-018-9602-2

[27] T. Q. Luong, V. Nguyen, Hydrothermal synthesis of superparamagnetic zinc–nickel ferrite nanoparticles, International Journal of Materials Research, 109 (**2018**) 6, 555–560, doi:10.3139/146.111629

[28] G. S Wang, Y. Y Ma, Y. Tong, X. Dong, M. Li, Solvothermal synthesis, characterization, and magnetorheological study of zinc ferrite nanocrystal clusters, Journal of Intelligent Material Systems and Structures, 28 (**2017**) 17, 2331–2338, doi:10.1177/1045389X16685449

[29] W. Shen, X. Q Chen, Y. Shi, M. Shi, H. ChenSynthesis of monodisperse and single-crystal Fe_3O_4 hollow spheres by a solvothermal approach, Materials Chemistry and Physics, 132 (**2012**), 987–992, doi:10.1016/j.matchemphys.2011.12.046